Histol Histopathol (2025) 40: 1295-1307

Histology and Histopathology
From Cell Biology to Tissue Engineering

ORIGINAL ARTICLE Open Access

TRIM22 mechanism promoting KAT2A ubiquitination degradation to regulate ferroptosis in hepatocellular carcinoma cell invasion and metastasis

Wei Wang[1]*, Xiaoshan Chen[2]* and Wei Wei[1]

[1]Department of Hepatobiliary and Pancreatic Surgery, Xiamen Humanity Hospital Fujian Medical University and [2]Department of Infectious Diseases, Zhongshan Hospital of Xiamen University, Xiamen, PR China

*Contributed equally

Summary. Objective. Hepatocellular carcinoma (HCC) is a highly fatal cancer. This study aims to investigate the underlying mechanism of tripartite motif-containing 22 (TRIM22) in HCC cell invasion and metastasis through the K (lysine) acetyltransferase 2A (KAT2A)/glutathione peroxidase 4 (GPX4) axis.

Methods. Human HCC cells BEL7405 were cultured *in vitro* and treated with MG-132, Ferrostain-1, pcDNA3.1-TRIM22, pcDNA3.1-KAT2A, or pcDNA3.1-NC. TRIM22-KAT2A interaction and KAT2A ubiquitination level, cell proliferation, invasion, migration, and histone H3 lysine 9 acetylation (H3K9ac) enrichment level on the GPX4 promoter were assessed by Co-IP, CCK-8, Transwell, and ChIP-qPCR assays. Mice were injected subcutaneously with Lv-oe-NC or Lv-oe-TRIM22 BEL7405 cells via the tail vein. Tumor proliferation and levels of TRIM22, KAT2A, GPX4, Fe^{2+}, malondialdehyde (MDA), reactive oxygen species (ROS), and glutathione (GSH) in tissues and cells were evaluated by immunohistochemistry, RT-qPCR, western blot, and kits.

Results. oe-TRIM22-treated BEL7405 cells exhibited increased TRIM22 expression, and abated KAT2A protein expression and malignant cell biological behaviors, which were partially reversed by upregulating KAT2A or suppressing ferroptosis. TRIM22 interacted with KAT2A, which was ubiquitinated to regulate GPX4 histone acetylation. TRIM22 overexpression elevated Fe^{2+}, MDA, and ROS levels and cell death, and diminished GSH, GPX4, and H3K9ac enrichment levels, whereas further overexpression of KAT2A brought about opposite trends. TRIM22 suppressed HCC growth and metastasis by mediating ferroptosis through the KAT2A/GPX4 axis.

Conclusions. TRIM22 promoted KAT2A ubiquitination degradation to reduce H3K9ac enrichment levels in the GPX4 promoter region, and facilitated ferroptosis, thereby inhibiting HCC cell invasion and metastasis and *in vivo* growth and metastasis.

Key words: Ubiquitination degradation, Ferroptosis, Tripartite motif-containing 22 (TRIM22), K (lysine) acetyltransferase 2A (KAT2A), Glutathione peroxidase 4 (GPX4), Invasion, Metastasis

Introduction

Hepatocellular carcinoma (HCC), arising from liver cells, accounts for roughly 90% of all cases of primary liver cancer (Chakraborty and Sarkar, 2022). HCC ranks in the top three leading causes of cancer-related mortality and is among the six most frequent malignancies globally (Ferlay et al., 2021). Unfortunately, HCC exhibits significant resistance to conventional cancer treatments, such as chemotherapy and radiotherapy, and its definitive diagnosis frequently arises in advanced stages, with an elevated probability of recurrence following curative treatment and a typically low overall survival rate (Song et al., 2021; Chakraborty and Sarkar, 2022). Therefore, accurate diagnosis and careful selection of target genes, along with the use of safe and efficient treatments such as immunotherapy or gene therapy, are crucial for the effective treatment of HCC (Chakraborty and Sarkar, 2022).

As an independent predictor of recurrence-free survival in HCC patients, E3 ubiquitin ligase tripartite motif-containing 22 (TRIM22) is lowly expressed in HCC tissues, and its overexpression has the potential to inhibit HCC cell proliferation (Lee et al., 2020; Wang et al., 2023). TRIM22 is crucial in inducing cell senescence in HCC cells, and the overexpression of TRIM22

Corresponding Author: Wei Wang, Department of Hepatobiliary and Pancreatic Surgery, Xiamen Humanity Hospital Fujian Medical University, No. 3777 Xianyue Road, Huli District, Xiamen 361000, Fujian Province, PR China. e-mail: Wanggweii02@163.com

www.hh.um.es. DOI: 10.14670/HH-18-856

specifically targets protein kinase B (AKT) phosphatase PHLPP2, resulting in cell senescence; as such, TRIM22 may function as a therapeutic target for cancer treatment (Kang et al., 2024). Nevertheless, little is known about the molecular mechanism underlying HCC cell invasion and metastasis. Notably, K (lysine) acetyltransferase 2A (KAT2A) is a histone acetyltransferase exerting a modulatory role in post-translational modification (Bondy-Chorney et al., 2019), and it is highly expressed in HCC tissues (Ling et al., 2018). A recent study suggested that the glycolytic enzyme fructose-1,6-bisphosphate aldolase B (ALDOB) inhibits the activity of KAT2A through direct interaction, leading to decreased histone H3 lysine 9 acetylation (H3K9ac), which subsequently suppresses HCC and TGF-β signaling (Yin et al., 2023). It has also been reported that TRIM22 interacts with KAT2A and facilitates its degradation via a ubiquitin-dependent mechanism, thus hindering malignant progression in melanoma cells, including proliferation, migration, and *in vivo* growth (Gu et al., 2023). Thus, TRIM22 may contribute to the degradation of the KAT2A protein by ubiquitination degradation, hence repressing the invasion and metastasis of HCC cells.

Importantly, ferroptosis has attracted a lot of interest because of its powerful effect on cancer cells, and its promotion has been shown to trigger innate and adaptive anti-tumor immune responses, contributing to the repression of HCC tumor growth (Cheu et al., 2023; Zheng et al., 2023). Recently, it has been documented that longevity assurance homologue 2 presents an inhibitory effect on the metastasis of tumor cells by affecting ferroptosis in the liver, thyroid, and breast cancer cells (Xu et al., 2024). Based on the above, we conjectured that TRIM22 could potentially degrade KAT2A through ubiquitination, diminishing H3K9ac enrichment levels in the glutathione peroxidase 4 (GPX4) promoter area to stimulate HCC cell ferroptosis, thereby preventing HCC cells from invasion and metastasis. However, relevant reports are limited. Our research mainly explores the mechanism by which TRIM22 facilitates the ubiquitination degradation of KAT2A to modulate ferroptosis in HCC invasion and metastasis, providing a foundation for the development of novel therapeutic targets and effective drugs for HCC.

Materials and methods

Ethics statement

The experiment was examined and approved by the Animal Ethics Committee of Xiamen Humanity Hospital Fujian Medical University, and the approved agreement was strictly abided by. We strictly adhered to the approved protocol, placing significant emphasis on reducing the number of animals used and mitigating their suffering.

Cell culture

Human HCC cells BEL7405 (Cat. No.: FH0834) were cultured in BEL7405 complete media (FH-BEL7405) in an incubator maintained at 95% humidity and 5% CO_2 at 37°C. Cells and culture media were obtained from Fuheng Biotechnology Co., Ltd. (Shanghai, China).

Cell line transfection and grouping

pcDNA3.1-TRIM22 (oe-TRIM22), pcDNA3.1-KAT2A (oe-KAT2A), and its control pcDNA3.1-NC (oe-NC) (GenePharma, Shanghai, China) were transfected into human HCC cell line BEL7405, all at a final transfection concentration of 100 ng/μL, using Lipofectamine® 2000 (Invitrogen, Carlsbad, CA, USA). The operation was performed under the product's manuals (Hou et al., 2018).

Cell grouping was as follows: Blank group (BEL7405 cells were cultured under standard conditions for 48 h), oe-NC group (BEL7405 cells were transfected with oe-NC for 48 h), oe-TRIM22 group (BEL7405 cells were transfected with oe-TRIM22 for 48 h); oe-TRIM22+MG-132 group [BEL7405 cells were delivered with oe-TRIM22 and simultaneously treated with 1.5 μmol/L MG-132 (HY-13259, MCE, Monmouth Junction, NJ, USA) for 48 h] (Wu et al., 2008); oe-TRIM22+vehicle group [BEL7405 cells were treated with oe-TRIM22 and the equal amount of MG-132 solvent [10% dimethyl sulfoxide (DMSO)+90% corn oil] simultaneously for 48 h]; oe-TRIM22+oe-NC group (BEL7405 cells underwent 48 h co-transfection with oe-TRIM22 and oe-NC); oe-TRIM22+oe-KAT2A group (BEL7405 cells underwent 48 h co-transfection with oe-TRIM22 and oe-KAT2A); oe-TRIM22+Fer-1 [BEL7405 cells were transfected with oe-TRIM22 and simultaneously treated with 1 μM Ferrostain-1 (HY-100579, MCE) for 48 h] (Li et al., 2023); and oe-TRIM22+vehicle group [BEL7405 cells were simultaneously cultured in the presence of oe-TRIM22 and an equivalent amount of Ferrostatin-1 solvent (10% DMSO+90% corn oil) for 48 h]. Each cell treatment was repeated three times independently.

Reverse transcription quantitative polymerase chain reaction (RT-qPCR)

Total RNA was extracted with TRIzol reagent (Invitrogen) and then reverse transcribed into cDNA using the PrimeScript RT reagent kit (Takara, Dalian, Liaoning, China). The TaqMan primers and probes used were sourced from Takara (Tokyo, Japan). qPCR was performed using the ABI PRISM 7900 sequence detection system of SYBR Green II (Takara). The PCR program was pre-denaturation at 95°C for 5 min, and 40 cycles of denaturation at 95°C for 15 s, annealing at 60°C for 20 s, and extension at 72°C for 35 s. Glyceraldehyde-3-phosphate dehydrogenase (GAPDH)

served as the internal reference; data were analyzed by the $2^{-\Delta\Delta Ct}$ method. The primer sequences were synthesized by Sangon Biotech Co., Ltd. (Shanghai, China), as shown in Table 1.

Western blot

Lysate (AR0107, Boster Biotechnology Co., Ltd., Wuhan, Hubei, China) was added to the cells to extract proteins, and the protein concentration was determined using the bicinchoninic acid kit (AR1189, Boster Biotechnology Co., Ltd.). Subsequently, an appropriate amount of loading buffer was added to the protein sample and denatured in a boiling water bath for 5 min. The denatured protein samples were then added to the loading wells, followed by sodium dodecyl sulfate-polyacrylamide gel electrophoresis to separate the proteins. Thereafter, the separated proteins were moved onto the polyvinylidene fluoride membrane via electrotransformation and then blocked in 3% bovine serum albumin for 2 h. After interaction with the primary antibodies (Table 2) at 4°C overnight, the samples were cultivated with goat anti-rabbit immunoglobulin G (IgG) H&L (HRP) at room temperature without light for 1h, followed by color development using the enhanced chemiluminescence working solution (AR1191, Boster Biotechnology Co., Ltd.). Image Pro Plus 6.0 (Media Cybernetics, Silver Spring, MD, USA) was used to quantify the gray value for western blot bands. GAPDH was regarded as an internal reference. The experiment was repeated thrice.

Co-immunoprecipitation (Co-IP) assay

Cell lysates were incubated with the antibodies anti-KAT2A (1:30, ab217876, Abcam, Cambridge, UK) or NC IgG (1:30, ab313801, Abcam), respectively, at 4°C overnight, followed by 2h incubation with PureProteome™ Protein A/G Mix Magnetic Beads (Merck Millipore, Billerica, MA, USA). The pre-cooled phosphate-buffered saline (PBS) was used to rinse agarose beads, before the elution of the binding protein. The precipitated protein was acquired via centrifugation and subsequently subjected to western blot assay to analyze the interaction between TRIM22 and KAT2A and the KAT2A ubiquitination level. The antibodies used for the western blot assay included an anti-TRIM22 antibody (1:1000, orb158646, Biorbyt, Waterbeach, Cambridge, UK) and anti-ubiquitin (1:30, ab209263, Abcam).

Cell counting kit-8 (CCK-8) assay

Differently treated cells (5×10^3 cells/well) were seeded in 96-well plates. Cell viability was assessed at 0, 12, 24, and 48 h using the CCK-8 kit (CA1210, Solarbio, Beijing, China). Afterward, 100 μL CCK-8 working solution was added to each well, and the cells were cultivated at 37°C for 2h. The microplate reader (Thermo Fisher Scientific, Waltham, MA, USA) was utilized to measure the optical density value at 450 nm.

Transwell assay

Cell invasion was detected using a Transwell chamber pre-filled with Matrigel matrix (BD Biosciences, Franklin Lakes, NJ, USA), and cell migration was evaluated using a Transwell chamber without the use of Matrigel. Before experiments, cells were subjected to 24 h culture in serum-free media and then resuspension in the medium containing 1% fetal bovine serum (FBS). The apical chamber was seeded with 1×10^5 cells, then 600 μL complete medium comprising 10% FBS was added to the basolateral chamber. Following incubation for 24 h, cells that failed to traverse the apical chamber were wiped with cotton swabs. Subsequently, cells were fixed with 4% paraformaldehyde and stained with hematoxylin (517-28-2, MACKLIN, Shanghai, China). Finally, three visual fields were randomly picked to observe and calculate the number of cells.

Lactate dehydrogenase (LDH) assay

The LDH assay kit (A020-2-2, Jiancheng Biological Engineering Research Institute, Nanjing, Jiangsu, China) was used to quantify cell death. Specific experimental steps were carried out according to the instructions (Li et al., 2022).

Chromatin immunoprecipitation (ChIP) assay

ChIP assay was performed utilizing the Simple ChIP Plus chromatin IP kit (#9005, Cell Signaling Technology, Beverly, MA, USA) as per the kit's instructions. Simply put, the sample was cut into pieces, crosslinked with 1.5% formaldehyde for 10 min at room temperature, and quenched for 5 min by the addition of glycine. Afterward, the samples were homogenized to create a single-cell suspension. Chromatin was incubated with 0.5 μL

Table 1. Primer sequences.

Gene	Forward 5'-3'	Reverse 5'-3'
TRIM22	GAGATGTCTGTGAGCACCAT	TCCTTGACCACCTCGTTT
KAT2A	TTCCGAGTGGAGAAGGACA	AGCATGGACAGGAATTTGG
GPX4	CCTTTGCCGCCTACTGAAG	GGTCGACGAGCTGAGTGTAG
GAPDH	CTCAGACACCATGGGGAAGGTGA	ATGATCTTGAGGCTGTTGTCATA

micrococcal nuclease for 20 min at 37°C, followed by ultrasonic treatment (a cycle of 100 W, 1 s on/5 s off; 10 cycles) to destroy the nuclear membrane. For IP, diluted chromatin was cultured in the presence of 3 μL normal IgG (control) (1:30, ab313801, Abcam) or 3 μL ac-H3K9 antibody (2 μg for 10^6 cells, ab4441, Abcam) overnight at 4°C in constant rotation, followed by 2 h incubation with 30 μL Protein G magnetic beads. Next, DNA was eluted from the magnetic beads, purified, and subjected to RT-qPCR using GPX4 (F: CCTTTGCCGCCTACTGAAG; R: GGTCGACGAGCTGAGTGTAG) primers. The ChIP-qPCR results were calculated as a percentage of input DNA (Lin et al., 2023).

Establishment of the HCC mouse model

A total of 18 BALB/c nude mice and 18 BALB/c mice (n=18, weighing 20±2 g), obtained from the Xiamen Institute of Food and Drug Quality Inspection [SYXK (Fujian) 2020-0009, Xiamen, Fujian, China], were fed in a standard specific pathogen-free animal room at 24±2°C, with 50±10% humidity, with a 12h light and dark cycle.

Lipofectamine® 2000 (Invitrogen) was used to transfect oe-TRIM22 lentivirus (Lv-oe-TRIM22) and its NC (Lv-oe-NC; GenePharma) into human HCC cells BEL7405 at a final transfecting concentration of 100 ng/μL following the product's instructions.

BALB/c nude mice were stochastically assigned to the following three groups (six mice per group): Model-1 group: BALB/c nude mice were subcutaneously inoculated with BEL7405 cells (5×10^6) on the back (Pang et al., 2023; Pittala et al., 2018); Lv-oe-NC-1 group: 5×10^6 of Lv-oe-NC-delivered BEL7405 cells were subcutaneously inoculated into the back of BALB/c nude mice; Lv-oe-TRIM22-1 group: BALB/c nude mice were injected subcutaneously on the back with 5×10^6 BEL7405 cells delivered with Lv-oe-TRIM22. After 10 days, the mice were euthanized with 150 mg/kg of 0.5% pentobarbital sodium (P3761, Sigma-Aldrich, St. Louis, MO, USA), and tumor tissues were collected. Tumor volumes were computed using the following formula: $\pi/6\times length\times width^2$ (Xian et al., 2021). In each group, half of the tumor tissues of nude mice were processed into paraffin sections for histological detection, and the remaining half were prepared as tissue homogenates and kept at -80°C for subsequent use.

BALB/c mice were randomly classified into three groups (six mice/group): Model-2 group: BALB/c mice were subjected to tail intravenous injection with 2×10^6 BEL7405 cells); Lv-oe-NC-2 group: BALB/c mice were injected with BEL7405 cells transfected with 2×10^6 Lv-oe-NC via the tail vein); and Lv-oe-TRIM22-2: BALB/c mice were injected with 2×10^6 of Lv-oe-TRIM22-transfected BEL7405 cells via the tail vein) (Yang et al., 2020). After 20 days, 150 mg/kg of 0.5% pentobarbital sodium (P3761, Sigma-Aldrich) was used to euthanize mice to examine the load of lung metastases. Lung metastases were counted by hematoxylin and eosin (H&E) staining (Yang et al., 2020).

mmunohistochemistry (IHC)

After careful rinsing with PBS, paraffin sections were placed in 0.01 M sodium citrate buffer (Sigma-Aldrich) and boiled to clear the antigens. Thereafter, sections were incubated in 3% H_2O_2 for 15 min at room temperature and blocked with 5% goat serum (SL038, Solarbio) for 30 min. Cells were mixed with anti-TRIM22 (1:500, ab224059, Abcam), anti-KAT2A (1:1000, ab254661, Abcam), anti-GPX4 (1:200, ab125066, Abcam), or anti-Ki67 (5 μg/mL, ab15580, Abcam) for overnight incubation at 4°C. After that, sections underwent interaction with goat anti-rabbit HRP (1:1000, ab214050, Abcam) secondary antibody at 37°C for 60 min. Finally, 3,3'-diaminobenzidine (DA1016, Solarbio) staining and hematoxylin (H8070, Solarbio) counterstaining were performed, and sections were observed and photographed under a microscope (Olympus, Tokyo, Japan). The quantitative analysis was conducted using Image-Pro Plus 6.0 (Media Cybernetics) (Wan et al., 2019).

Determination of Fe^{2+}, malondialdehyde (MDA), glutathione (GSH), and reactive oxygen species (ROS)

The levels of Fe^{2+}, MDA, GSH, and ROS were measured using the iron test kit (ab83366, Abcam), MDA assay kit (ab118970, Abcam), reduced GSH assay kit (BC1175, Solarbio), and ROS assay kit (ab186029, Abcam), respectively, following the manufacturers' protocols.

H&E staining

Tissues received 24h fixation in 4% para-formaldehyde. Then, the samples were embedded in paraffin, sliced into 4-μm-thick sections, and dyed with the HE Kit (C0105S, Beyotime, Shanghai, China). Specific operations were executed as per the provided manuals. Thereafter, five visual fields were chosen at random, and histopathological alterations in lung tissues were observed using a microscope (Olympus) (Xu et al., 2021a ; Gao et al., 2023).

Statistical analysis

Data analysis was implemented using GraphPad Prism

Table 2. Antibodies used for western blot.

Antibodies	Cat. No. & Company	Dilution ratio
TRIM22	orb158646, Biorbyt	1/1000
KAT2A	ab217876, Abcam	1/1000
GPX4	orb340797, Biorbyt	1/2000
GAPDH	ab181602, Abcam	1/1000
IgG H&L (HRP)	ab6721, Abcam	1/2000

8.01 statistical software (GraphPad Software Inc., San Diego, CA, USA). Data were tested to be normally distributed by the Kolmogorov-Smirnov test, and the results are expressed as mean±standard deviation (SD). One-way analysis of variance (ANOVA) was used for multi-group comparisons, followed by Tukey's multiple comparison test. *p*-values below 0.05 were considered significant.

Results

TRIM22 downregulated KAT2A protein levels in a ubiquitination-degradation manner, and suppressed the proliferation, invasion, and migration of HCC cells

Firstly, we cultured human HCC BEL7405 cells *in*

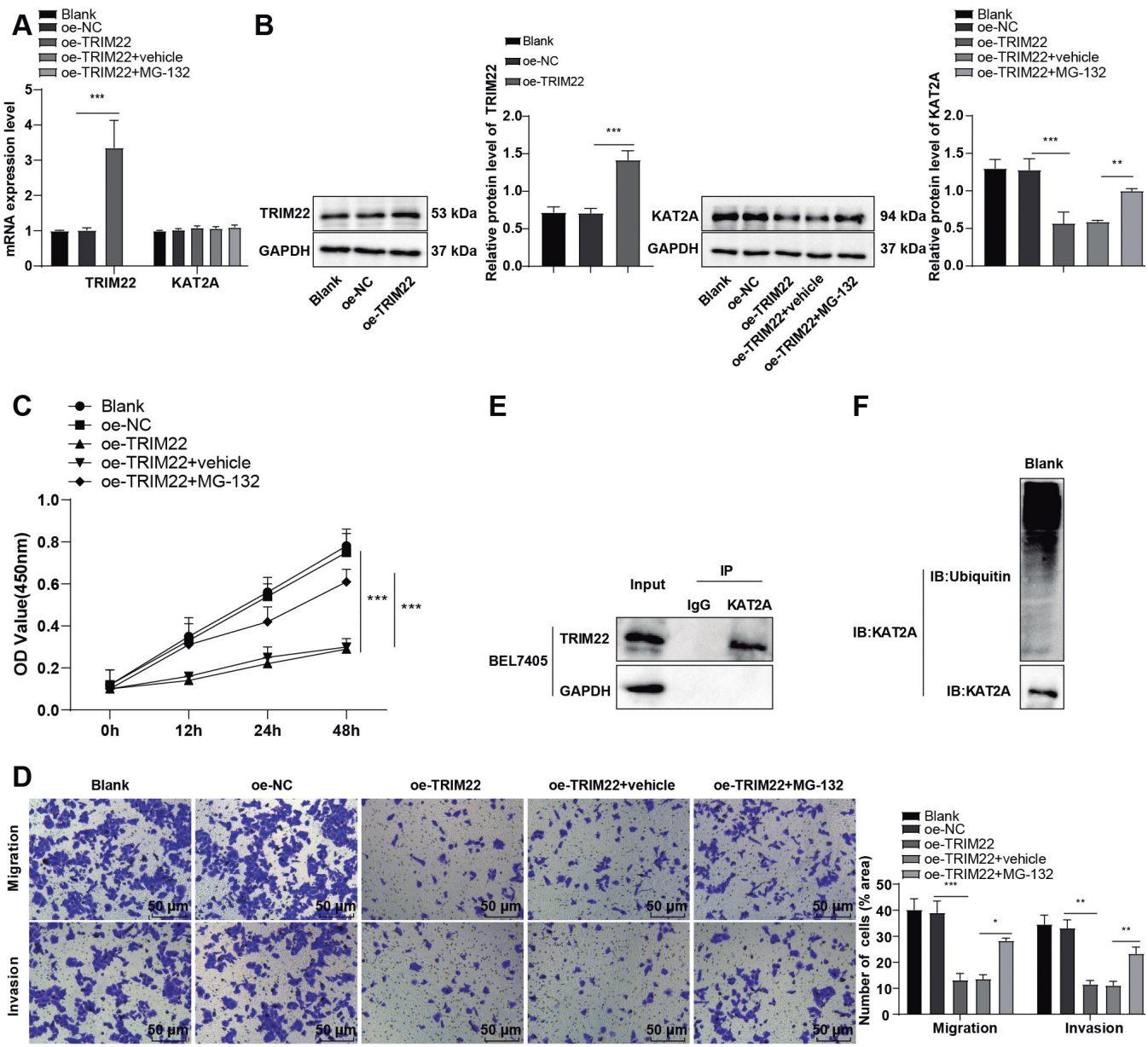

Fig. 1. TRIM22 downregulated KAT2A protein levels in a ubiquitination-degradation manner and repressed HCC cell invasion, proliferation, and migration. **A.** RT-qPCR to determine TRIM22 and KAT2A mRNA levels. **B.** Western blot to measure TRIM22 and KAT2A protein levels. **C.** CCK-8 detection to assess cell proliferation. **D.** Transwell assay to evaluate cell invasion and migration. **E.** Co-IP assay to detect the interaction between TRIM22 and KAT2A. **F.** Co-IP assay to detect the ubiquitination level of KAT2A. The cell experiment was repeated three times independently, and the data are expressed as mean±SD. One-way ANOVA was used for data comparisons between multiple groups, and Tukey's multiple comparison test was used for the *post-hoc* test. **p*<0.05, ***p*<0.01, ****p*<0.001.

vitro and transfected the cells with oe-TRIM22 and its NC. As detected by RT-qPCR and western blot, compared with the oe-NC group, TRIM22 expression in the oe-TRIM22 group was increased ($p<0.001$), the level of KAT2A protein was decreased ($p<0.001$), and KAT2A mRNA expression did not vary significantly ($p>0.05$) (Fig. 1A,B). Additionally, the oe-TRIM22 group showed diminished cell proliferation ($p<0.001$) (Fig. 1C) and reduced cell invasive and migratory capacities ($p<0.01$) (Fig. 1D) relative to the oe-NC group. Co-IP assay revealed that there was an interplay between TRIM22 and KAT2A (Fig. 1E), and KAT2A was ubiquitinated (Fig. 1F). Later, we treated BEL7405 cells with oe-TRIM22 and the ubiquitin-proteasome inhibitor MG-132. The results elicited no distinct change in the expression of KAT2A mRNA ($p>0.05$); yet, there was an elevation in the expression of KAT2A protein ($p<0.01$) and promotion in cell proliferation, invasion, and migration ($p<0.05$) (Fig. 1A-D). These findings indicated that TRIM22 curbed the malignant phenotypes of HCC cells by downregulating KAT2A protein levels in a ubiquitination-degradation manner.

KAT2A upregulation partly counteracted the inhibitory effects of TRIM22 on HCC cell invasion, proliferation, and migration

Furthermore, we used oe-TRIM22 and oe-KAT2A to concurrently transfect human HCC BEL7405 cells. The results delineated that KAT2A expression was increased ($p<0.01$) (Fig. 2A,B), cell proliferation was promoted ($p<0.001$) (Fig. 2C), and cell migratory and invasive

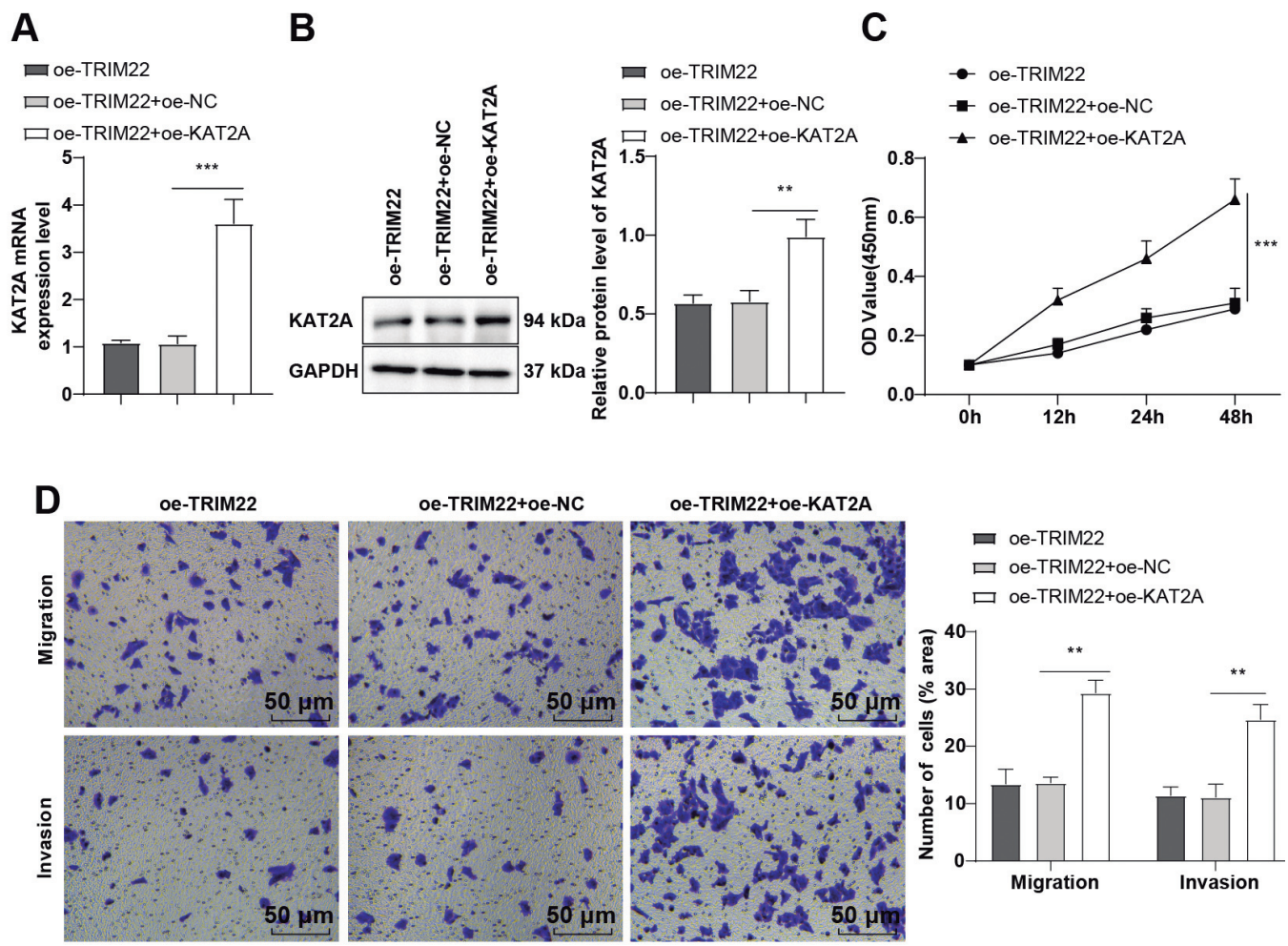

Fig. 2. Upregulation of KAT2A partially annulled the suppressive effects of TRIM22 on the proliferation, invasion, and migration of HCC cells. **A.** KAT2A mRNA level was determined by RT-qPCR. **B.** KAT2A protein level was measured by western blot. **C.** Cell proliferation was evaluated by the CCK-8 assay. **D.** Cell invasion and migration were assessed by Transwell assay. The cell experiment was repeated three times independently. The data are expressed as the mean±SD. One-way ANOVA was used for data comparisons, and Tukey's multiple comparison test was used for the *post-hoc* test. $^{**}p<0.01$, $^{***}p<0.001$.

capacities were intensified (p<0.01) (Fig. 2D). These results manifested that the upregulation of KAT2A partly abrogated the inhibitory effects of TRIM22 on the migration, invasion, and proliferation abilities of HCC cells.

TRIM22 inhibited H3K9ac enrichment in the GPX4 promoter region by regulating KAT2A, thus stimulating ferroptosis in HCC cells

We detected the levels of Fe^{2+}, GSH, MDA, and ROS in HCC cells using reagent kits. In comparison with the oe-NC group, MDA, Fe^{2+}, and ROS levels showed incremental trends (p<0.01), whereas GSH levels were on a downward trend (p<0.001) (Fig. 3A) in the oe-TRIM22 group. The results of the LDH assay illustrated that cell death was increased in the oe-TRIM22 group *versus* the oe-NC group (p<0.01) (Fig. 3B). Concerning the results of RT-qPCR and western blot, compared with oe-NC group, the expression of GPX4 in the oe-TRIM22 group was diminished (p<0.001) (Fig. 3C,D). Moreover, the oe-TRIM22 group displayed lower H3K9ac enrichment levels in the GPX4 promoter region than the oe-NC group (p<0.01) (Fig. 3E), as was shown by the ChIP assay. In addition, we further used oe-KAT2A and oe-TRIM22 to concomitantly treat BEL7405 cells, which resulted in diminished levels of Fe^{2+}, ROS, and MDA (p<0.05), heightened levels of GSH and GPX4 (all p<0.01), suppressed cell death (p<0.01), and increased H3K9ac enrichment levels in the GPX4 promoter region (p<0.05) (Fig. 3A-E). In a word, TRIM22 suppressed the enrichment of H3K9ac in the GPX4 promoter region by modulating KAT2A, which in turn accelerated ferroptosis in HCC cells.

Inhibition of ferroptosis partially annulled the inhibitory effects of TRIM22 on the malignant behaviors of HCC cells

Subsequently, we simultaneously treated BEL7405 cells with oe-TRIM22 and the ferroptosis inhibitor Ferrostain-1. The levels of Fe^{2+}, MDA, and ROS dropped (p<0.05), GSH levels rose (p<0.05), cell death was abated (p<0.05), cell proliferation was boosted (p<0.01), and cell invasion and migration were also reinforced (p<0.05) (Fig. 4A-D). The data evidenced that the repression mediated by TRIM22 on HCC cell malignant behaviors was partially negated by ferroptosis inhibition.

TRIM22 repressed the growth of HCC in vivo by mediating ferroptosis through the KAT2A/GPX4 axis

Finally, we performed xenograft tumor experiments in nude mice via subcutaneous injection of HCC cells (BEL7405) transfected with Lv-oe-NC or Lv-oe-TRIM22 lentivirus. Mice in the Lv-oe-TRIM22-1 group had diminished tumor volumes (p<0.05) (Fig. 5A). Furthermore, as reflected by the IHC assay, in contrast to

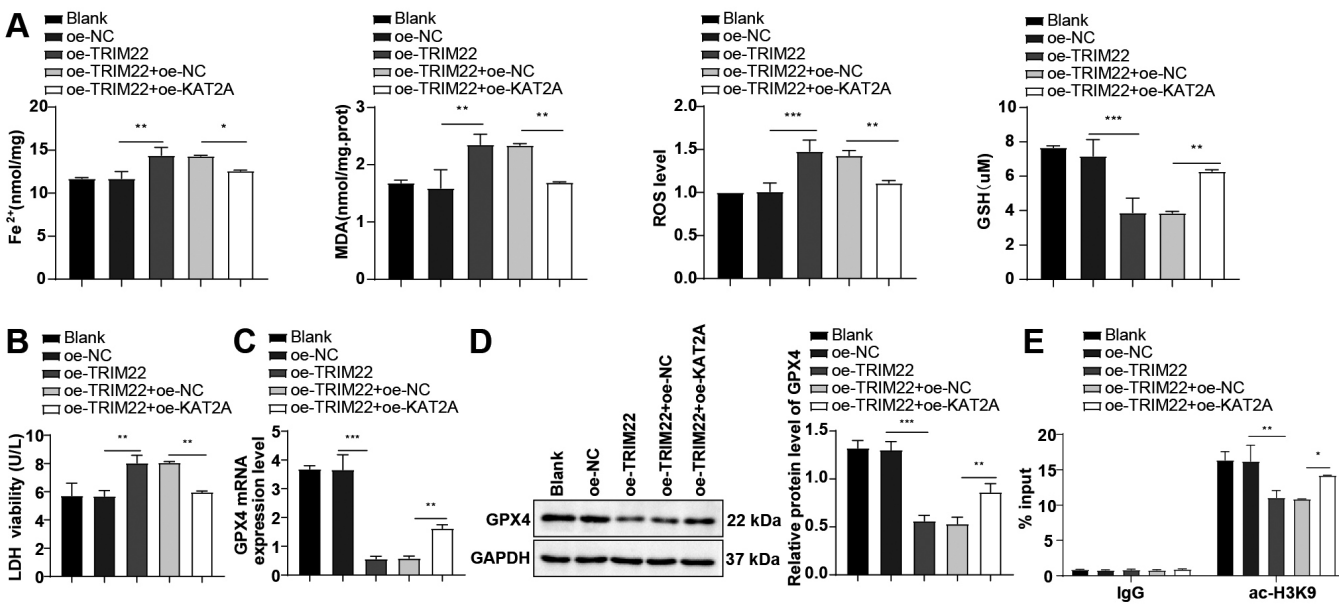

Fig. 3. TRIM22 boosted ferroptosis in HCC cells by modulating KAT2A to mediate H3K9ac in the GPX4 promoter region. **A.** Fe^{2+}, ROS, GSH, and MDA levels in cells were determined using kits. **B.** LDH assay to evaluate cell death. **C.** GPX4 mRNA level was measured using RT-qPCR. **D.** GPX4 protein level was determined by western blot. **E.** Enrichment level of H3K9ac on the GPX4 promoter was assessed by ChIP assay. The cell experiment was repeated three times independently. Data are exhibited as mean±SD. One-way ANOVA was used for multi-group data comparisons and Tukey's multiple comparison test was used for the *post-hoc* test. *p<0.05, **p<0.01, ***p<0.001.

the Lv-oe-NC-1 group, TRIM2 expression in tumor tissues was elevated ($p<0.05$), and KAT2A and GPX4 expression levels were abated ($p<0.05$) (Fig. 5B) in the Lv-oe-TRIM22-1 group. Compared with the Lv-oe-NC-1 group, the Lv-oe-TRIM22-1 group showed elevated Fe^{2+}, MDA, and ROS levels ($p<0.01$), as well as reduced GSH levels ($p<0.05$) (Fig. 5C) in tumor tissues. Additionally, significantly decreased levels of Ki67-positive cells were found in the Lv-oe-TRIM22-1 group *versus* the Lv-oe-NC-1 group ($p<0.05$) (Fig. 5D).

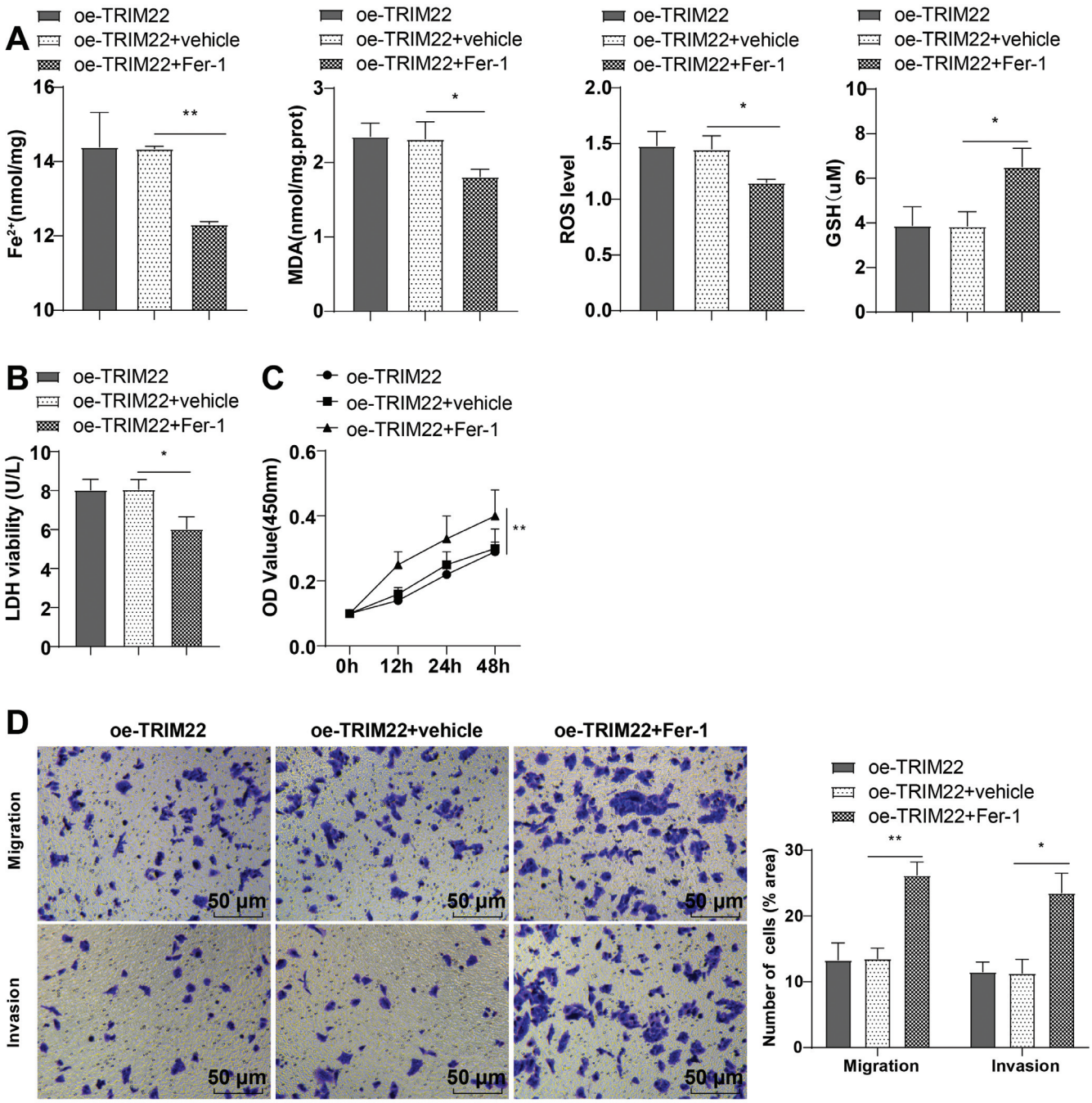

Fig. 4. Inhibition of ferroptosis partly abolished the inhibitory effects of TRIM22 on the proliferation, invasiveness, and migration of HCC cells. **A.** MDA, ROS, GSH, and Fe^{2+} levels were tested using kits. **B.** LDH assay to assess cell death. **C.** CCK-8 assay to evaluate cell viability. **D.** Cell invasion and migration were evaluated by the Transwell assay. The repetition of independent cell experiments was performed thrice. Data are exhibited as mean±SD. One-way ANOVA was employed for multi-group data comparisons and Tukey's multiple comparison test was used for the *post-hoc* test. *$p<0.05$, **$p<0.01$.

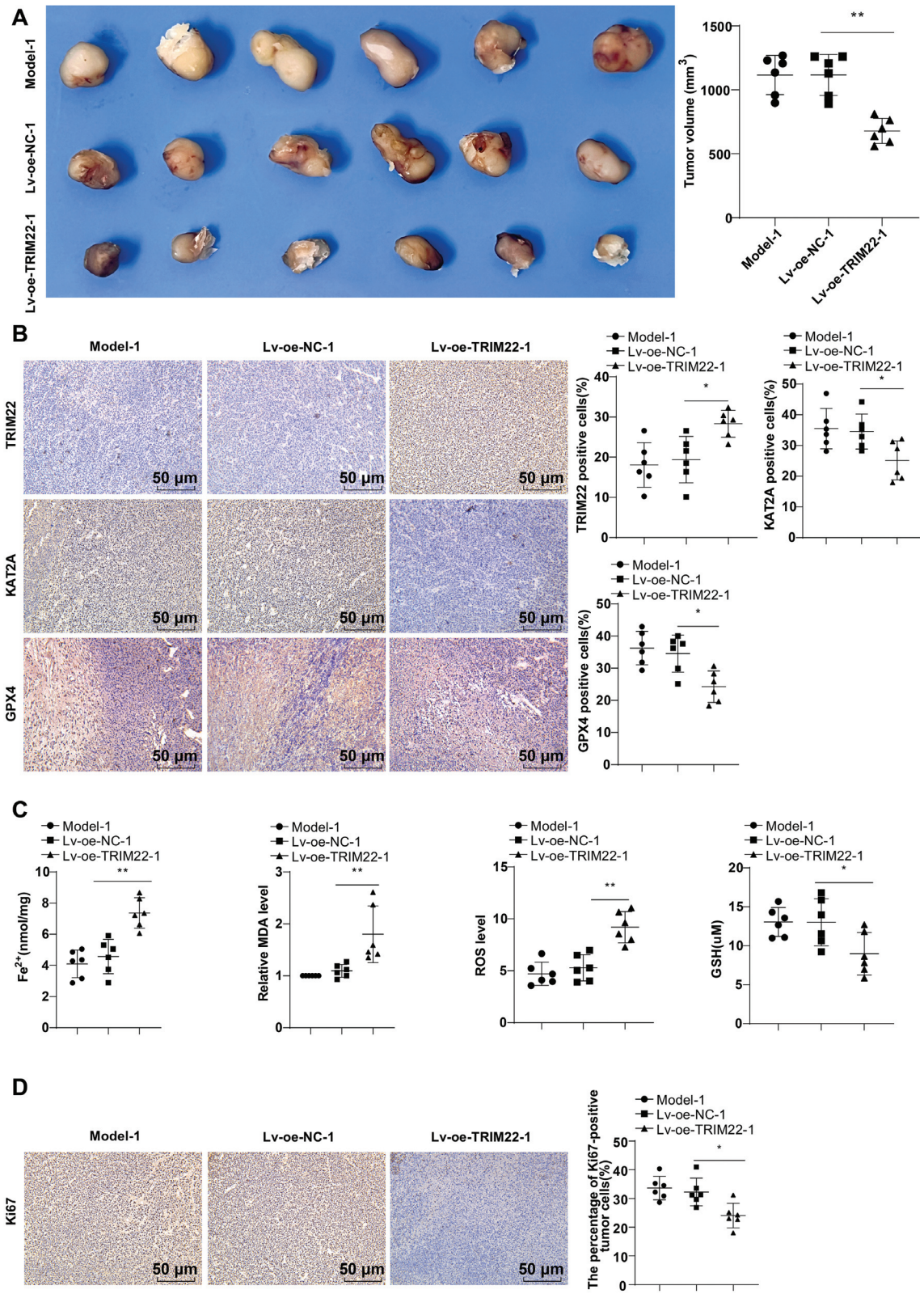

Fig. 5. TRIM22 restricted HCC *in vivo* growth by mediating ferroptosis via the KAT2A/GPX4 axis. **A.** Representative graph of tumor size and volume changes. **B.** The expression levels of TRIM22, GPX4, and KAT2A in tissues were determined by IHC. **C.** The levels of MDA, GSH, Fe^{2+}, and ROS in tissues were measured using kits. **D.** Tumor proliferation was evaluated by Ki67 IHC staining. n=6. Data are presented as mean±SD. Multi-group data comparisons were performed by one-way ANOVA and Tukey's multiple comparison test was used for the *post-hoc* test. *p<0.05, **p<0.01.

Overall, TRIM22 suppressed the growth of HCC *in vivo* by mediating ferroptosis through the KAT2A/GPX4 axis.

TRIM22 suppressed the in vivo metastasis of HCC by targeting the KAT2A/GPX4 axis

To further verify whether TRIM22 could repress the metastasis of HCC *in vivo* via the KAT2A/GPX4 axis, we injected 2×10^6 BEL7405 cells that were transfected with Lv-oe-NC or Lv-oe-TRIM22 lentivirus into BALB/c mice via the tail vein. We found that the Lv-oe-TRIM22-2 group displayed fewer lung metastases in the lungs of mice than the Lv-oe-NC-2 group ($p<0.05$) (Fig. 6A). Also, we determined the expression levels of TRIM22, KAT2A, and GPX4 in lung tissues by IHC. In comparison with the Lv-oe-NC-2 group, mice in the Lv-oe-TRIM22-2 group exhibited increased TRIM2 expression ($p<0.05$), as well as decreased KAT2A and GPX4 expression levels in lung tissues ($p<0.05$) (Fig. 6B). These findings demonstrated that TRIM22 restrained the metastasis of HCC *in vivo* through the KAT2A/GPX4 axis.

Discussion

The preferable therapeutic approach for HCC is surgery due to its potential to attain long-term survival and cure; however, a significant proportion of HCC patients in China have progressed to an advanced to intermediate stage of the illness, rendering surgical intervention impracticable (Zhou and Song, 2021). As such, understanding the molecular mechanisms of HCC is crucial for the timely identification, diagnosis, and treatment of this condition (Zhou et al., 2018). Interestingly, TRIM proteins have been demonstrated to be implicated in cell proliferation, cell death, and treatment resistance in HCC (Lu et al., 2022). Our study provided valuable evidence regarding the target gene TRIM22, highlighting its potential for better treatment strategies for patients with HCC. This study demonstrated that TRIM22 reduced invasion and metastasis of HCC cells by facilitating the ubiquitination degradation of KAT2A to inhibit ferroptosis.

As a family of E3 ubiquitin ligases, TRIMs can promote proteasome-mediated protein degradation (Zhao et al., 2021; Zou et al., 2021). Prior studies have

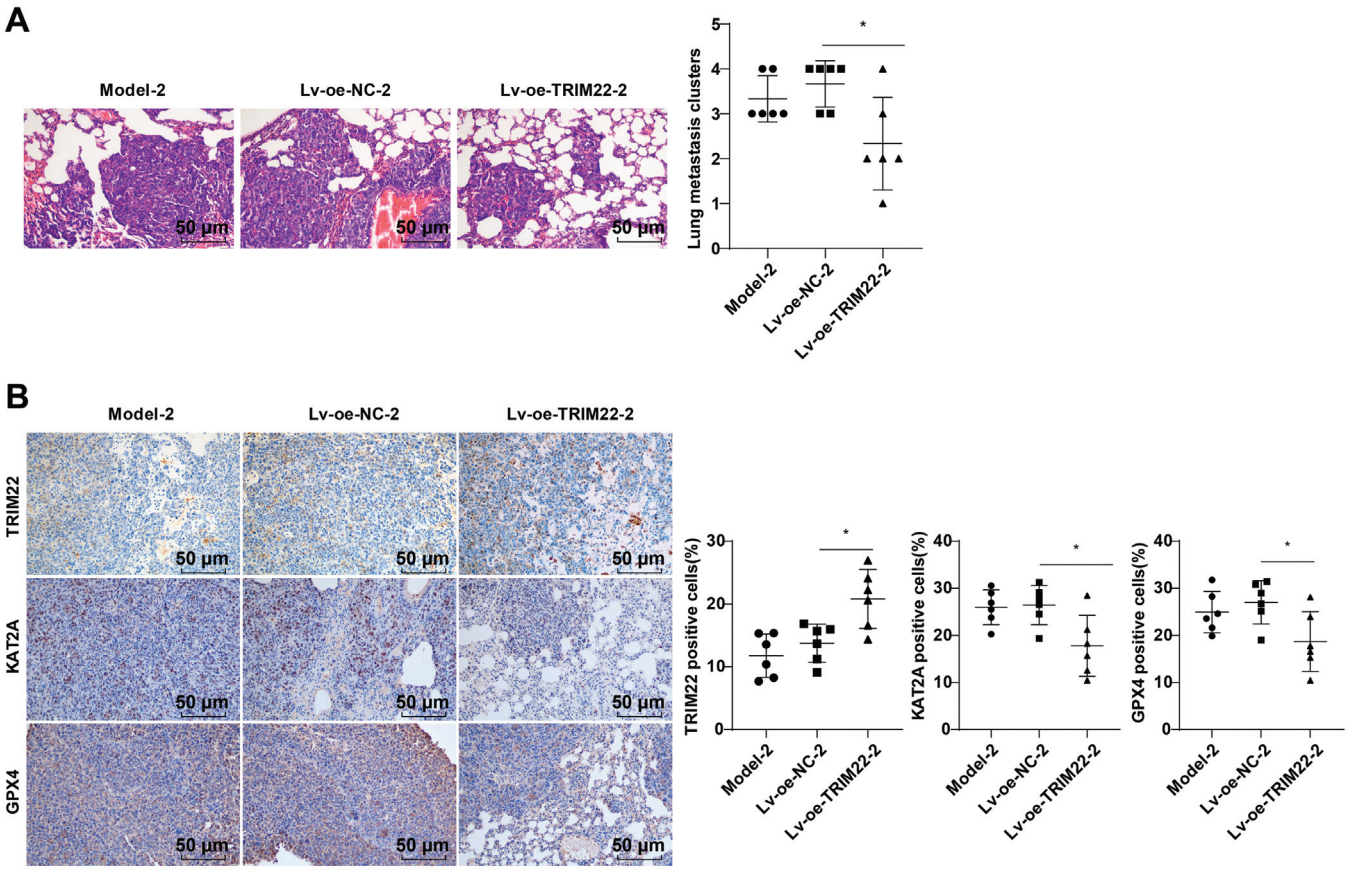

Fig. 6. TRIM22 inhibited HCC metastasis *in vivo* via the KAT2A/GPX4 axis. **A.** H&E staining to count lung metastatic tumors. **B.** The expression levels of GPX4, KAT2A, and TRIM22 in lung tissues were determined by IHC. n=6. Data are denoted as mean±SD. Multi-group data comparisons were conducted using one-way ANOVA and Tukey's multiple comparison test was used for the *post-hoc* test. *$p<0.05$.

provided insight into the various functions of TRIM22 in the immune system, especially its ability to identify viral agents, inhibit their reproduction, enhance immune responses, and contribute to ubiquitination processes (Pagani et al., 2021; Reddi et al., 2021). Recent data demonstrated that TRIM22 modulates the proteasomal degradation of PHLPP2, thereby regulating cancer cell senescence in HCC cells, suggesting that TRIM22 may represent a viable therapeutic target in the treatment of HCC (Kang et al., 2024). Functionally, TRIM22 mediates the ubiquitination of the KAT2A protein through its interactions with KAT2A, a confirmed target of TRIM22, and the absence of TRIM22 leads to a significant increase in the level of KAT2A protein in melanoma (Gu et al., 2023). Of interest, TRIM22 overexpression exerts inhibitory effects on the growth, colony formation, and metastasis of gastric cancer cells (Zhou et al., 2021). Liu et al. reported that TRIM22 impedes osteosarcoma progression by engaging with and enhancing the ubiquitination and breakdown of nuclear factor erythroid 2-related factor 2 (Liu et al., 2022). Notwithstanding, the essential role of the succinyltransferase activity of KAT2A in stimulating proliferation or migration cannot be underestimated (Lu et al., 2021). Specifically, KAT2A mediates H3K79 succinylation to affect the stability of β-catenin and accelerate the proliferation and invasion of pancreatic cancer cells (Tong et al., 2020). The inhibition of KAT2A brought about a reduction in the invasive and migratory capabilities of lung cancer cells (Qu et al., 2024). Similar to these previous studies, we found that oe-TRIM22 induced downregulated KAT2A protein levels, cell migration, invasion, and growth by interacting with and potentiating KAT2A ubiquitination degradation. Beyond that, KAT2A is markedly increased in multiple cancer types, enhancing proliferation and exacerbating the invasion and migration of cancer cells (Sandoz et al., 2019; Jiang et al., 2020). Unsurprisingly, we also noted that KAT2A upregulation partially invalidated the suppressive impacts of TRIM22 on the invasion, migration, and proliferation of HCC cells.

Ferroptosis is an iron-dependent cell death process, characterized by an elevation in Fe^{2+} buildup within cells, ROS accumulation, and the occurrence of lipid peroxidation like MDA, which exerts vital modulatory effects on the occurrence and development of cancer, such as HCC (Dixon et al., 2014; Yang and Stockwell, 2016; Xu et al., 2021b). As reported, KAT2A can modulate GPX4 levels to stimulate the malignant phenotypes of colorectal cancer cells and induce ferroptosis (Xu et al., 2024). In a similar light, our *in vitro* experiments validated that overexpressing TRIM22 limited the histone acetylation of GPX4 by regulating KAT2A, thus speeding up ferroptosis in HCC cells, as evidenced by elevated levels of ROS, Fe^{2+}, and MDA, along with lessened GSH. Moreover, we conducted the analysis of co-treatment with oe-TRIM22 and Ferrostatin-1 in BEL7405 cells. It is interesting to note that Ferrostatin-1 partly counteracted the inhibition of HCC cell growth, invasion, and metastasis induced by TRIM22 overexpression. Similarly, recent research indicated that repression of ferroptosis by Ferrostatin-1 nullifies all-trans retinoic acid-suppressed HCC cell growth, migration, and invasiveness (Sun et al., 2022). Another study reported that the ferroptosis inhibitor, Ferrostatin-1, partially counteracts the repression of HCC cell growth mediated by rhamnazin (Mei et al., 2022). Consequently, repressing ferroptosis partly annulled TRIM22-induced suppression of the malignant behaviors of HCC cells. Additionally, *in vivo* assays were further conducted to assess the effects of TRIM22 by regulating KAT2A/GPX4 in HCC *in vivo* growth and metastasis. There is convincing proof that KAT2A deletion greatly suppresses renal carcinoma cell growth and distal metastasis in the A498 metastatic model (Guo et al., 2021). Besides, the knockdown of GPX4 by RSL3 has been documented to augment the anticancer properties of cisplatin by suppressing tumor growth via ferroptosis (Zhang et al., 2020). According to the findings of *in vivo* tumor formation experiments, we uncovered that Lv-oe-TRIM22-transfected BALB/c nude mice exhibited reduced tumor volumes, decreased KAT2A and GPX4 expression levels, augmented ferroptosis, as well as reduced Ki67-positive cell levels and lung metastases. Based on the evidence, TRIM22 hindered HCC growth and metastasis *in vivo* by expediting ferroptosis via the KAT2A/GPX4 axis.

In conclusion, the present data showed that TRIM22 suppressed ferroptosis by enhancing KAT2A ubiquitination degradation to modulate ferroptosis, thereby diminishing the invasion and metastasis of HCC cells. In addition, TRIM22 mediated ferroptosis through the KAT2A/GPX4 axis, thereby curbing the growth and metastasis of HCC *in vivo*. However, there were some limitations in the current study in that we did not investigate the mechanism by which TRIM22 simulated KAT2A ubiquitination degradation to inhibit ferroptosis, thus reducing HCC cell invasion and metastasis at the clinical level. Therefore, in the future, our focus will be on identifying the upstream or downstream target of TRIM22 to promote the ubiquitination degradation of KAT2A and studying the role of other related signal pathways in HCC. Alternatively, we may begin by studying autophagy, mitochondrial autophagy, or oxidative stress.

Acknowledgment. Not applicable.

Funding. None.

Ethics statement. The experiment was examined and approved by the Animal Ethics Committee of Xiamen Humanity Hospital Fujian Medical University, and the approved agreement was strictly abided by. We strictly adhered to the approved protocol, placing significant emphasis on reducing the number of animals used and mitigating their suffering.

Conflict of Interest Statement. The authors have no conflicts of interest to declare.

Data Availability Statement. All data generated or analyzed during this study are included in this article. Further inquiries can be directed to the corresponding author.

References

Bondy-Chorney E., Denoncourt A., Sai Y. and Downey M. (2019). Nonhistone targets of KAT2A and KAT2B implicated in cancer biology. Biochem. Cell Biol. 97, 30-45.

Chakraborty E. and Sarkar D. (2022). Emerging therapies for hepatocellular carcinoma (HCC). Cancers 14, 2798

Cheu J.W., Lee D., Li Q., Goh C.C., Bao M.H., Yuen V.W., Zhang M.S., Yang C., Chan C.Y.-K., Tse A.P.-W., Sit G.F.-W., Liu C.X., Ng I.O.-L., Wong C.-M. and Wong C.C. (2023). Ferroptosis suppressor protein 1 inhibition promotes tumor ferroptosis and anti-tumor immune responses in liver cancer. Cell. Mol. Gastroenterol. Hepatol. 16, 133-159.

Dixon S.J., Patel D.N., Welsch M., Skouta R., Lee E.D., Hayano M., Thomas A.G., Gleason C.E., Tatonetti N.P., Slusher B.S. and Stockwell B.R. (2014). Pharmacological inhibition of cystine-glutamate exchange induces endoplasmic reticulum stress and ferroptosis. Elife 3, e02523.

Ferlay J., Colombet M., Soerjomataram I., Parkin D.M., Pineros M., Znaor A. and Bray F. (2021). Cancer statistics for the year 2020: An overview. Int. J. Cancer 149, 778-779.

Gao K., Yu X., Li F., Huang Y., Liu J., Liu S., Lu L., Yang R. and Wang C. (2023). Qishen granules regulate intestinal microecology to improve cardiac function in rats with heart failure. Front. Microbiol. 14, 1202768.

Gu X., Min W., Zeng Y., Fan N. and Qian Q. (2023). Aberrant KAT2A accumulations render TRIM22-low melanoma sensitive to Notch1 inhibitors via epigenetic reprogramming. J. Transl. Med. 21, 443.

Guo Y., Liu B., Liu Y., Sun W., Gao W., Mao S., and Chen L. (2021). Oncogenic chromatin modifier KAT2A activates MCT1 to drive the glycolytic process and tumor progression in renal cell carcinoma. Front. Cell Dev. Biol. 9, 690796.

Hou Y., Che D., Ma P., Zhao T., Zeng Y. and Wang N. (2018). Anti-pseudo-allergy effect of isoliquiritigenin is MRGPRX2-dependent. Immunol. Lett. 198, 52-59.

Jiang Y., Guo X., Liu L., Rode S., Wang R., Liu H. and Yang Z.Q. (2020). Metagenomic characterization of lysine acetyltransferases in human cancer and their association with clinicopathologic features. Cancer Sci. 111, 1829-1839.

Kang D., Hwang H.J., Baek Y., Sung J.Y., Kim K., Park H.J., Ko Y.-G., Kim Y.-N. and Lee J.S. (2024). TRIM22 induces cellular senescence by targeting PHLPP2 in hepatocellular carcinoma. Cell Death Dis. 15, 26.

Lee Y.S., Ko E., Yoon E.L., Jung Y.K., Kim J.H., Seo Y.S., Yim H.J., Kim K.-H., Kwon S.Y., Yeon J.E., Um S.H. and Byun K.S. (2020). Multiplexed proteomic approach for identification of serum biomarkers in hepatocellular carcinoma patients with normal AFP. J. Clin. Med. 9, 323.

Li Y., Sun X., Zhuang J., Wang J. and Yang C. (2022). Donepezil ameliorates oxygen-glucose deprivation/reoxygenation-induced cardiac microvascular endothelial cell dysfunction through PARP1/NF-κB signaling. Mol. Med. Rep. 25, 121.

Li D., Wang Y., Dong C., Chen T., Dong A., Ren J., Li W., Shu G., Yang J., Shen W., Qin L., Hu L. and Zhou J. (2023). CST1 inhibits ferroptosis and promotes gastric cancer metastasis by regulating GPX4 protein stability via OTUB1. Oncogene 42, 83-98.

Lin Y., Lin A., Cai, L., Huang W., Yan S., Wei Y., Ruan X., Fang W., Dai X., Cheng J., Zhang J., Chen W., Ye Q., Chen X. and Zhang J. (2023). ACSS2-dependent histone acetylation improves cognition in mouse model of Alzheimer's disease. Mol. Neurodegener. 18, 47.

Ling Z.A., Xiong D.D., Meng R.M., Cen J.M., Zhao N., Chen G., Li R.-L. and Dang, Y.W. (2018). LncRNA NEAT1 promotes deterioration of hepatocellular carcinoma based on *in vitro* Experiments, Data Mining, and RT-qPCR Analysis. Cell Physiol. Biochem. 48, 540-555.

Liu W., Zhao Y., Wang G., Feng S., Ge X., Ye W., Wang Z., Zhu Y., Cai W., Bai J. and Zhou X. (2022). TRIM22 inhibits osteosarcoma progression through destabilizing NRF2 and thus activation of ROS/AMPK/mTOR/autophagy signaling. Redox Biol. 53, 102344.

Lu D., Song Y., Yu Y., Wang D., Liu B., Chen L., Li X., Li Y., Cheng L., Lv F., Zhang P. and Xing Y. (2021). KAT2A-mediated AR translocation into nucleus promotes abiraterone-resistance in castration-resistant prostate cancer. Cell Death Dis. 12, 787.

Lu K., Pan Y., Huang Z., Liang H., Ding Z.Y. and Zhang B. (2022). TRIM proteins in hepatocellular carcinoma. J. Biomed. Sci. 29, 69.

Mei F., Liu Y. and Zheng S. (2022). Rhamnazin inhibits hepatocellular carcinoma cell Aggressiveness *in Vitro* via Glutathione peroxidase 4-Dependent ferroptosis. Tohoku J. Exp. Med. 258, 111-120.

Pagani I., Poli G. and Vicenzi E. (2021). TRIM22. A multitasking antiviral factor. Cells 10, 1864.

Pang N., Hu Q., Zhou Y., Xiao Y., Li W., Ding Y., Chen Y., Ye M., Pei L., Li Q., Gu Y., Sun Y., Fang E.F., Chen M., Zhang Z. and Yang L. (2023). Nicotinamide adenine dinucleotide precursor suppresses hepatocellular cancer progression in mice. Nutrients 15, 1447.

Pittala S., Krelin Y. and Shoshan-Barmatz V. (2018). Targeting liver cancer and associated pathologies in mice with a mitochondrial VDAC1-based peptide. Neoplasia 20, 594-609.

Qu A., Han B., Hua M., Wang C. and Li T. (2024). SF3B4 down-regulation restrains lung adenocarcinoma tumorigenesis via 5' alternative splicing of KAT2A. Sci. Rep. 14, 30.

Reddi T.S., Merkl P.E., Lim S.Y., Letvin N.L. and Knipe D.M. (2021). Tripartite Motif 22 (TRIM22) protein restricts herpes simplex virus 1 by epigenetic silencing of viral immediate-early genes. PLoS Pathog. 17, e1009281.

Sandoz J., Nagy Z., Catez P., Caliskan G., Geny S., Renaud J.B., Concordet J.-P., Poterszman A., Tora L., Egly J.M., Le May N. and Coin F. (2019). Functional interplay between TFIIH and KAT2A regulates higher-order chromatin structure and class II gene expression. Nat. Commun. 10, 1288.

Song Z.B., Yu Y., Zhang G.P. and Li S.Q. (2021). Genomic instability of mutation-derived gene prognostic signatures for hepatocellular carcinoma. Front. Cell Dev. Biol. 9, 728574.

Sun Y., He Y., Tong J., Liu D., Zhang H., He T. and Bi Y. (2022). All-trans retinoic acid inhibits the malignant behaviors of hepatocarcinoma cells by regulating ferroptosis. Genes Dis, 9, 1742-1756.

Tong Y., Guo D., Yan D., Ma C., Shao F., Wang Y., Luo S., Lin L., Tao J., Jiang Y., Lu Z. and Xing D. (2020). KAT2A succinyltransferase activity-mediated 14-3-3zeta upregulation promotes beta-catenin stabilization-dependent glycolysis and proliferation of pancreatic carcinoma cells. Cancer Lett. 469, 1-10.

Wan X., Huang H.C., Wang X.P., Hu Z.H., Liu K.Y. and Huang D.B. (2019). Euonymus alatus and its monomers alleviate liver fibrosis both in mice and LX2 cells by blocking TbetaR1-Smad2/3 and TNF-alpha-NF-kappaB pathways. Am. J. Transl. Res. 11, 106-119.

Wang H., Yang C., Li D., Wang R., Li Y. and Lv L. (2023). Bioinformatics analysis and experimental validation of a novel autophagy-related signature relevant to immune infiltration for recurrence prediction after curative hepatectomy. Aging 15, 2610-

2630.

Wu W.K., Sung J.J., Yu L. and Cho C.H. (2008). Proteasome inhibitor MG-132 lowers gastric adenocarcinoma TMK1 cell proliferation via bone morphogenetic protein signaling. Biochem. Biophys. Res. Commun. 371, 209-214.

Xian D., Niu L., Zeng J. and Wang L. (2021). LncRNA KCNQ1OT1 secreted by tumor Cell-derived exosomes mediates immune escape in colorectal cancer by regulating PD-L1 ubiquitination via MiR-30a-5p/USP22. Front. Cell Dev. Biol. 9, 653808.

Xu S., Wu B., Zhong B., Lin L., Ding Y., Jin X., Huang Z., Lin M., Wu H. and Xu D. (2021a). Naringenin alleviates myocardial ischemia/reperfusion injury by regulating the nuclear factor-erythroid factor 2-related factor 2 (Nrf2) /System xc-/ glutathione peroxidase 4 (GPX4) axis to inhibit ferroptosis. Bioengineered 12, 10924-10934.

Xu Z., Peng B., Liang Q., Chen X., Cai Y., Zeng S., Gao K., Wang X., Yi Q., Gong Z. and Yan Y. (2021b). Construction of a ferroptosis-related nine-lncRNA signature for predicting prognosis and immune response in hepatocellular carcinoma. Front. Immunol. 12, 719175.

Xu Z., Wang X., Yu P., Zhang Y., Huang L., Mao E. and Han Y. (2024). Lysine acetyltransferase KAT2A modulates ferroptosis during colorectal cancer development. Scand J. Gastroenterol. 59, 437-444.

Yang W.S. and Stockwell B.R. (2016). Ferroptosis: Death by lipid peroxidation. Trends Cell Biol. 26, 165-176.

Yang L.Y., Luo Q., Lu L., Zhu W.W., Sun H.T., Wei R., Lin Z.-F., Wang X.-Y., Wang C.-Q., Lu M., Jia H.-L., Chen J.-H., Zhang J.-B. and Qin L.X. (2020). Increased neutrophil extracellular traps promote metastasis potential of hepatocellular carcinoma via provoking tumorous inflammatory response. J. Hematol. Oncol. 13, 3.

Yin C., Zhang C., Wang Y., Liu G., Wang N., Liang N., Zhang L., Tu Q., Lv J., Jiang H., Ma H., Du C., Li M., He X., Chen S., Guo J., Li S., Qin J., Li N., Tao Y. and Yin H. (2023). ALDOB/KAT2A interactions epigenetically modulate TGF-β expression and T cell functions in hepatocellular carcinogenesis. Hepatology 81, 77-93.

Zhang X., Sui S., Wang L., Li H., Zhang L., Xu S. and Zheng X. (2020). Inhibition of tumor propellant glutathione peroxidase 4 induces ferroptosis in cancer cells and enhances anticancer effect of cisplatin. J. Cell. Physiol. 235, 3425-3437.

Zhao J., Cai B., Shao Z., Zhang L., Zheng Y., Ma C., Yi F., Liu B. and Gao C. (2021). TRIM26 positively regulates the inflammatory immune response through K11-linked ubiquitination of TAB1. Cell Death Differ. 28, 3077-3091.

Zheng Y., Wang Y., Lu Z., Wan J., Jiang L., Song D., Wei C., Gao C., Shi G., Zhou J., Fan J., Ke A., Zhou L. and Cai J. (2023). PGAM1 inhibition promotes HCC ferroptosis and synergizes with Anti-PD-1 immunotherapy. Adv. Sci. 10, e2301928.

Zhou H. and Song T. (2021). Conversion therapy and maintenance therapy for primary hepatocellular carcinoma. Biosci. Trends 15, 155-160.

Zhou L., Du Y., Kong L., Zhang X. and Chen Q. (2018). Identification of molecular target genes and key pathways in hepatocellular carcinoma by bioinformatics analysis. Onco. Targets Ther. 11, 1861-1869.

Zhou Z., Gao W., Yuan B., Zhang S., Wang K. and Du T. (2021). TRIM22 inhibits the proliferation of gastric cancer cells through the Smad2 protein. Cell Death Discov. 7, 234.

Zou D.B., Mou Z., Wu W. and Liu H. (2021). TRIM33 protects osteoblasts from oxidative stress-induced apoptosis in osteoporosis by inhibiting FOXO3a ubiquitylation and degradation. Aging Cell 20, e13367.

Accepted November 29, 2024